



Available online at www.sciencedirect.com

SciVerse ScienceDirect

journal homepage: www.elsevier.com/locate/bbe



Original Research Article

Planar arm movement trajectory formation: An optimization based simulation study

Matjaž Zadavec*, Zlatko Matjačić

University Rehabilitation Institute, Republic of Slovenia

ARTICLE INFO

Article history:

Received 14 November 2012

Accepted 22 December 2012

Available online 16 May 2013

Keywords:

Trajectory planning

Stroke rehabilitation

Upper extremity

Muscle tightness

Dynamic optimization

Rehabilitation robotics

ABSTRACT

Rehabilitation of post stroke patients with upper extremity motor deficits is typically focused on relearning of motor abilities and functionalities requiring interaction with physiotherapists and/or rehabilitation robots. In a point-to-point movement training, the trajectories are usually arbitrarily determined without considering the motor impairment of the individual. In this paper, we used an optimal control model based on arm dynamics enabling also incorporation of muscle functioning constraints (i.e. simulation of muscle tightness) to find the optimal trajectories for planar arm reaching movements. First, we tested ability of the minimum joint torque cost function to replicate the trajectories obtained in previously published experimental trials done by neurologically intact subjects, and second, we predicted the optimal trajectories when muscle constraints were modeled. The resulting optimal trajectories show considerable similarity as compared to the experimental data, while on the other hand, the muscle constraints play a major role in determination of the optimal trajectories for stroke rehabilitation.

© 2013 Naęcz Institute of Biocybernetics and Biomedical Engineering. Published by Elsevier Urban & Partner Sp. z o.o. All rights reserved.

1. Introduction

Upper extremity motor deficits are prevalent post stroke requiring efficient motor rehabilitation, which is typically focused on relearning of motor abilities and functionalities, often necessitating one-on-one manual interaction with physiotherapists and/or rehabilitation robots. In recent years, rehabilitation robots made their way to clinical practice as they can apply high-intensity, repetitive, task-specific, interactive treatment with objective and reliable means of monitoring of patient progress. Robot-aided therapy can also evaluate patient's movements and assist them in moving the upper extremity through a predetermined trajectory during a given motor task. In current rehabilitation robot assisted arm training

predominantly straight line trajectories connecting the starting and ending points of upper extremity movement are being used. This might be to a large extent based on predictions of the minimum jerk trajectory formation model, proposed by [1–3], which is, however, valid only under assumptions that no constraints either in the movement space, i.e. boundaries of range of motion (ROM), or the musculo-skeletal system are present. In contrast, some experimental [4–6] and theoretical [5,7,8] results suggest curved paths when either of constraints are invoked, especially when the target point is at the boundary of arm's ROM or in the case if the path is long-distanced.

Furthermore, symmetrical velocity profiles predicted by the minimum jerk models are not always consistent with the experimental trajectories. For instance, it has been demonstrated that in the case of slow movements, the maximum

* Corresponding author at: University Rehabilitation Institute, Republic of Slovenia.

E-mail address: matjaz.zadavec@ir-rs.si (M. Zadavec).

velocity is shifted toward the beginning of the movements, and toward the end in the case of ballistic movements [9]. Hence, different character of movement as well as the functional (dis)ability of the arm would suggest different cost function (rather than minimum jerk), which may be more appropriate to determine the optimal trajectory. Furthermore, one may expect entirely different arm trajectories when muscle spasticity or any kind of arm weakness is considered. More natural cost function in rehabilitation robotics supported movement training, where muscle weakness and muscle tightness pose considerable constraints, would be one related to required joint torques, since the rehabilitation robot needs to supply a “missing” joint torques.

The aim of this paper was first to develop an optimal control model based on arm dynamics enabling also incorporation of altered muscle functioning constraints, which can simulate arm tightness. With our proposed model we compared the experimental data of the arm reaching movements performed by neurologically intact population and described in the previous study [4] to test the ability of the selected cost function minimizing a sum of squared torques in the shoulder and elbow, to predict trajectories at boundaries of the ROM and long-distanced trajectories. Since the experimental trials were done by neurologically intact subjects, we first optimized the movements based on two-link model dynamics, where muscle constraints (i.e. passive muscle forces) were not included in the model. To find the optimal trajectory, the first-order gradient algorithm with the minimum jerk trajectory as an initial guess was used. In the optimization process, we used exactly the same

physical parameters of the planar two-link human arm model, the start and end points, and the movement duration as described and reported in the compared study. We then incorporated stiffness-based muscle tightness emulations to investigate its influence on the minimum torque based solution implying different trajectories to be practiced in the neurologically impaired central nervous system.

2. Methods

2.1. Human arm model

We modeled a human arm that consisted of two links, where the first link is upper arm, while the second link is consisted of forearm and hand. This 2 DOF human arm model has two rotational joints representing the shoulder ($i = 1$) and elbow ($i = 2$) joints. The model is simplified for planar arm reaching and does not contain the gravitational vector. A schematic model of the human arm is shown in Fig. 1(a), where all the variables and most of the arm parameters are indicated. The shoulder joint is located at the position $(0, 0)$ of Cartesian coordinate system as shown in Fig. 1. This model also contains six muscles attaching to the arm links as shown in Fig. 1(b). Two monoarticular muscles causing torque in the shoulder joint (1-*pectoralis major* and 2-*posterior deltoid*), two monoarticular muscles around elbow joint (3-*brachialis* and 4-*lateral head of triceps brachii*), and two biarticular muscles (5-*biceps brachii* and 6-*long head of triceps*) are shown.

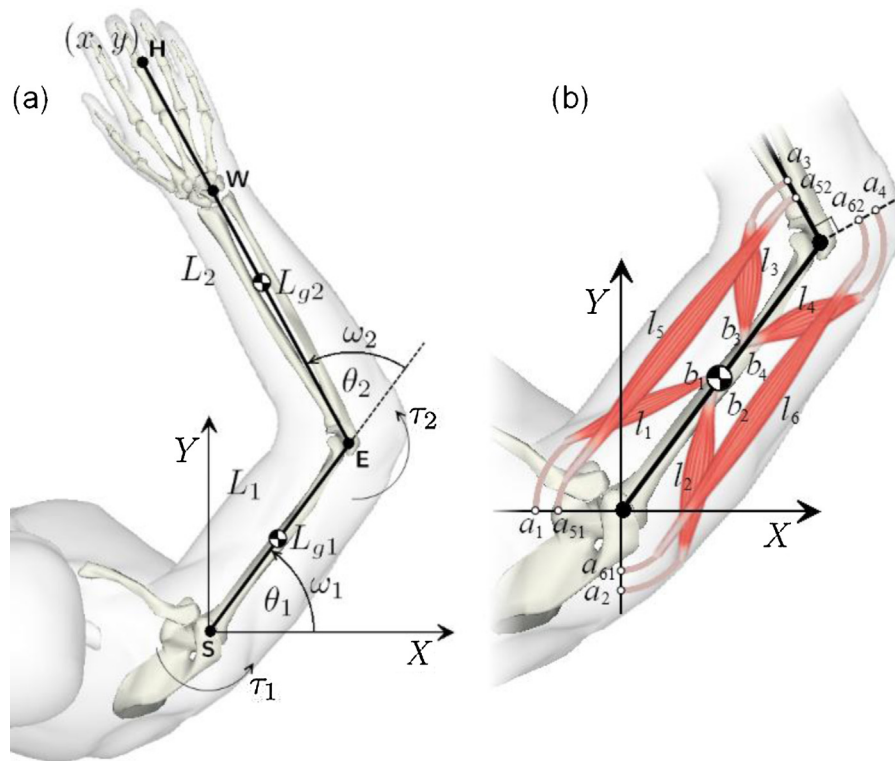


Fig. 1 – Planar human arm model. (a) Kinematic model of human arm modeled as a planar two-link manipulator. (b) Six muscle model with four monoarticular muscles (1-*pectoralis major*, 2-*posterior deltoid*, 3-*brachialis*, 4-*lateral head of triceps brachii*) and two biarticular muscles (5-*biceps brachii*, 6-*long head of triceps*).

2.1.1. The kinematics of links

The hand position of the two-link arm, which is defined in Cartesian coordinate system as the coordinates (x, y) , can be expressed by joint angles (θ_1, θ_2) , yielding forward kinematics:

$$\begin{bmatrix} x \\ y \end{bmatrix} = \begin{bmatrix} L_1 \cos \theta_1 + L_2 \cos(\theta_1 + \theta_2) \\ L_1 \sin \theta_1 + L_2 \sin(\theta_1 + \theta_2) \end{bmatrix}. \quad (1)$$

The inverse kinematics relations can be written as

$$\begin{bmatrix} \theta_1 \\ \theta_2 \end{bmatrix} = \begin{bmatrix} \arctan2(y, x) - \arccos\left(\frac{r^2 + L_1^2 - L_2^2}{2L_1 r}\right) \\ \pi - \arccos\left(\frac{L_1^2 + L_2^2 - r^2}{2L_1 L_2}\right) \end{bmatrix}, \quad (2)$$

where $r = \sqrt{x^2 + y^2}$ and $\arctan2(y, x) = \arctan(y/x) + \text{sgn}(y) \times (1 - \text{sgn}(x))\pi/2$.

2.1.2. Arm dynamics

The manipulator dynamics were modeled with the Lagrangian formulation without using potential energy. The manipulator dynamics are specified by (3), where $\tau = [\tau_1 \ \tau_2]^T$ are torques around the shoulder and elbow joints, $\tau_{\text{muscles}} = [\tau_{1, \text{muscles}} \ \tau_{2, \text{muscles}}]^T$ are joint torques due to passive muscle forces, $\theta = [\theta_1 \ \theta_2]^T$ are joint angles, $\dot{\theta} = [\dot{\omega}_1 \ \dot{\omega}_2]^T$ are angle velocities, and $\ddot{\theta} = [\ddot{\omega}_1 \ \ddot{\omega}_2]^T$ are angle accelerations.

$$M(\theta)\ddot{\theta} + C(\theta, \dot{\theta})\dot{\theta} + B\dot{\theta} = \tau + \tau_{\text{muscles}}. \quad (3)$$

The manipulator inertia matrix M , Coriolis and centrifugal matrix C , and viscosity matrix B are given as follows

$$M(\theta) = \begin{bmatrix} \alpha + 2\beta \cos \theta_2 & \delta + \beta \cos \theta_2 \\ \delta + \beta \cos \theta_2 & \delta \end{bmatrix}, \quad (4)$$

$$C(\theta, \dot{\theta}) = \begin{bmatrix} -\beta\dot{\theta}_2 \sin \theta_2 & -\beta(\dot{\theta}_1 + \dot{\theta}_2) \sin \theta_2 \\ \beta\dot{\theta}_1 \sin \theta_2 & 0 \end{bmatrix}, \quad (5)$$

$$B = \begin{bmatrix} b_{11} & b_{12} \\ b_{21} & b_{22} \end{bmatrix} \quad (6)$$

with the following constants

$$\alpha = I_1 + I_2 + m_1 L_{g1}^2 + m_2 (L_1^2 + L_{g2}^2), \quad (7)$$

$$\beta = m_2 L_1 L_{g2}, \quad (8)$$

$$\delta = I_2 + m_2 L_{g2}^2. \quad (9)$$

2.1.3. Muscle modeling

The muscle lengths $l = [l_1, l_2, l_3, l_4, l_5, l_6]^T$ are expressed as follows:

$$\begin{bmatrix} l_1 \\ l_2 \\ l_3 \\ l_4 \\ l_5 \\ l_6 \end{bmatrix} = \begin{bmatrix} -a_1 \theta_1 + \sqrt{b_1^2 - a_1^2} + a_1 \left(\pi - \arccos \frac{a_1}{b_1} \right) \\ a_2 \theta_1 + \sqrt{b_2^2 - a_2^2} + a_2 \left(\frac{\pi}{2} - \arccos \frac{a_2}{b_2} \right) \\ -a_3 \theta_2 + \sqrt{b_3^2 - a_3^2} + a_3 \left(\pi - \arccos \frac{a_3}{b_3} \right) \\ a_4 \theta_2 + \sqrt{b_4^2 - a_4^2} + a_4 \left(\frac{\pi}{2} - \arccos \frac{a_4}{b_4} \right) \\ a_{51} \left(\frac{\pi}{2} - \theta_1 \right) + \sqrt{L_1^2 + (a_{51} - a_{52})^2} + a_{52} \left(\frac{\pi}{2} - \theta_2 \right) \\ a_{61} \theta_1 + \sqrt{L_1^2 + (a_{61} - a_{62})^2} + a_{62} \theta_2 \end{bmatrix}, \quad (10)$$

where a_{1-4} , b_{1-4} , a_{51} , a_{52} , a_{61} and a_{62} represent the moment levers of each muscle. The levers are assumed to be constant in the arm's workspace, independent of the joint angles. The moment lever matrix is then given by

$$W^T = \begin{bmatrix} -a_1 & a_2 & 0 & 0 & -a_{51} & a_{61} \\ 0 & 0 & -a_3 & a_4 & -a_{52} & a_{62} \end{bmatrix}. \quad (11)$$

In our model, we used only passive muscle force of Hill-type model for force generation [10] to simulate muscle tightness conditions. Since the muscles can only exert positive forces, the passive muscle force is given by (12), considering inequality constraints. The shape of the exponential was determined by the variable K_{sh} and the scaling factor F_0 defined the nominal passive muscle force.

$$F(l) = \begin{cases} 0, & l < l_0 \\ \frac{F_0}{e^{K_{sh}} - 1} (e^{(K_{sh}(l-l_0))/(0.5l_0)} - 1), & l \geq l_0 \end{cases} \quad (12)$$

The passive muscle force begins to work at the nominal muscle length l_0 onwards, while it remains zero up to l_0 . Fig. 2 shows the relation between the normalized passive muscle force and the muscle length, where two different muscle conditions are represented: normal (solid line) and muscle tightness (dashed line). The difference between these two conditions is in the nominal muscle length, where passive muscle force under muscle tightness conditions begins to work at a shorter muscle length (i.e. at $l_{0, \text{m.t.}}$) than under normal conditions (i.e. at $l_{0, \text{normal}}$). This relation is given by following inequality

$$l_{0, \text{m.t.}} < l_{0, \text{normal}}. \quad (13)$$

The relation of the joint torque vector τ_{muscles} and the muscle force vector $F = [F_1, F_2, F_3, F_4, F_5, F_6]^T$ is defined by

$$\tau_{\text{muscles}} = W^T F(l). \quad (14)$$

2.1.4. Muscle static field

To represent the characteristics of arm's muscle tightness in the workspace, the joint torques (i.e. the static joint torques τ_{static}) were calculated from (3), where all angle velocities and angle accelerations contributions were excluded. The muscle static field is then defined as $\sqrt{\tau_{\text{static}}^T \tau_{\text{static}}}$, where the static joint torques are expressed as follows

$$\tau_{\text{static}}(\theta) = -W^T F(l(\theta)). \quad (15)$$

2.1.5. Model parameters

Since our first goal was to compare the results of our study with the experimental results made by Suzuki et al., we used exactly the same physical parameters of human arm, measured and determined in [4]. In the experimental procedures of the comparative study, six male subjects (age 20–34 years) participated. All subjects were right-handed and free of known musculoskeletal and neurological abnormalities [4]. The representative subject from the experiment was 34 years old, 1.78 m high and 80 kg weighing male participant. The estimated lengths and the inertial parameters of two segments are given in Table 1. The length of upper arm segment L_1 was defined as a distance between the shoulder joint center (S) and the elbow joint center (E), and the length of

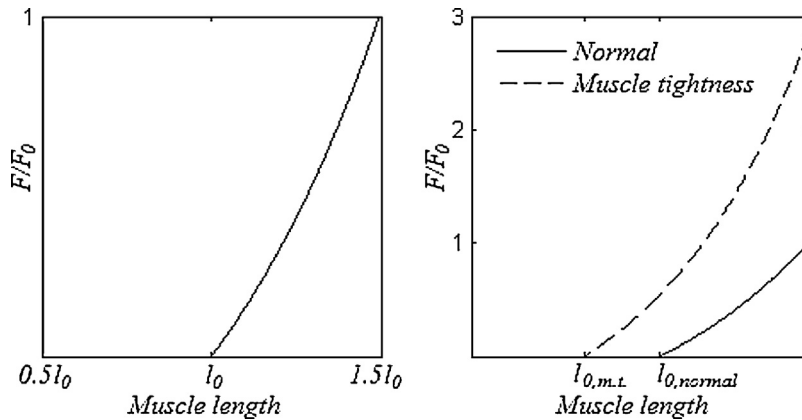


Fig. 2 – The relation between normalized passive muscle force and muscle length. The exponential function of passive force begins at the nominal muscle length l_0 (left graph), but in the case of muscle tightness, the passive muscle force already begins to work at a shorter muscle length: $l_{0,m.t.} < l_{0,normal}$ (right graph).

forearm segment including hand L_2 as a distance between the elbow joint center (E) and the distal end of the first phalanx of the middle finger (H). The position of the center-of-mass (COM) of upper arm and forearm is defined as a proportional distance from the proximal joint center to the COM with the respect to the total segment distance as shown in Fig. 1, labeled L_{g1} and L_{g2} . The mass and inertia parameters of human arm were used on the basis of the studies [11–14] on the human body characteristics. The numerical constants of the viscosity matrix are given by (16). These constants, used for movements in the horizontal plane, were experimentally determined by [5].

$$B = \begin{bmatrix} 0.74 & 0.10 \\ 0.10 & 0.82 \end{bmatrix} [Nm s] \tag{16}$$

The positions at which the muscles connect the bones were set according to [15], except that we avoid the muscle singularities by setting the muscle torque levers to be constant (Table 2). The nominal length of each muscle, at which passive muscle force begins to work, was defined in a way that the entire workspace of the arm (i.e. $-20^\circ < \theta_1 < 120^\circ$ and $0^\circ < \theta_2 < 135^\circ$) was systematically examined by setting out the extent to which each muscle length changes. Then, the average value of the recorded muscle lengths was defined as its nominal length under the normal muscle condition. In our optimization process, the nominal lengths under the muscle tightness conditions were set to $l_{0,m.t.} = 0.9 \cdot l_{0,normal}$. The

variable K_{sh} , which defines the shape of exponential passive muscle force and the scaling factor F_0 were defined arbitrary. The values of nominal muscle forces and the nominal muscle lengths under the normal and muscle tightness conditions are shown in Table 3.

2.2. Initial and final postures

Nine points were selected in the horizontal plane of 2 DOF right arm model [4]. Three starting (S_1, S_2, S_3) and three ending points (T_1, T_2, T_3) of the hand position were defined as a determination of the shoulder and elbow joint angles, θ_1 and θ_2 . The two joint angles are used to describe the initial and final arm postures as shown in Fig. 3. The initial postures were defined at different shoulder angles with a constant elbow joint angle of 90° , positioned in the middle of working area, while the final postures were determined by the placement of the three targets at the edge of arm workspace, also with different shoulder angles and the constant elbow joint angle of 25° . All six selected arm postures and the corresponding hand positions in Cartesian coordinate system are represented in Table 4 and Fig. 3. Thereby, the shoulder joint motion had different directions and magnitudes, while the elbow joint had constant extensions of 65° from all start to end point directions (Table 5). All possible combinations were separated in three parts. Part A represents combinations of initial and final

Table 1 – Physical parameters of two-segment human arm model were used for the dynamic optimization. Estimated lengths and inertial parameters of a representative subject (age 34 years, height 1.78 m, weight 80 kg) were used on the basis of point-to-point movement experiment.

Parameter	Shoulder joint ($i = 1$)	Elbow joint ($i = 2$)
Length L_i [m]	0.298	0.419
Mass m_i [kg]	2.089	1.912
Center of mass L_{gi} [m]	0.152	0.181
Moment of inertia I_i [kg m ²]	0.0159	0.0257

Table 2 – Muscle torque levers, connections points and passive force shape parameter. The shape of exponential muscle passive force was set by variable K_{sh} .

0.055	a_{1-2} [m]
0.045	a_{4-5} [m]
0.055	a_{51} [m]
0.045	a_{52} [m]
0.055	a_{61} [m]
0.045	a_{62} [m]
0.080	b_{1-2} [m]
0.120	b_{3-4} [m]
1	K_{sh}

Table 3 – Nominal muscle forces and nominal muscle lengths. We set the relation between muscle tightness and normal nominal muscle lengths to $l_{0,m.t.} = 0.9l_{0,normal}$.

Muscle	F_0 [N]	$l_{0,normal}$ [m]	$l_{0,m.t.}$ [m]
Pectoralis major	120	0.1382	0.1244
Posterior deltoid	120	0.1478	0.1330
Brachialis	120	0.1462	0.1316
Triceps brachii (lateral head)	120	0.1816	0.1634
Biceps brachii	100	0.3542	0.3188
Triceps (long head)	100	0.3992	0.3593

Table 4 – Initial and final arm postures defined by shoulder (θ_1) and elbow (θ_2) joint angles, with the corresponding hand positions in Cartesian coordinate system, which determine the three starting (S_1, S_2, S_3) and three ending points (T_1, T_2, T_3), i.e. targets.

Target	Arm posture		Hand position
	θ_1 (°)	θ_2 (°)	(x, y) [m]
S_1	110	90	(-0.50, 0.14)
S_2	65	90	(-0.25, 0.45)
S_3	20	90	(0.14, 0.50)
T_1	95	25	(-0.24, 0.66)
T_2	50	25	(0.30, 0.63)
T_3	5	25	(0.66, 0.24)

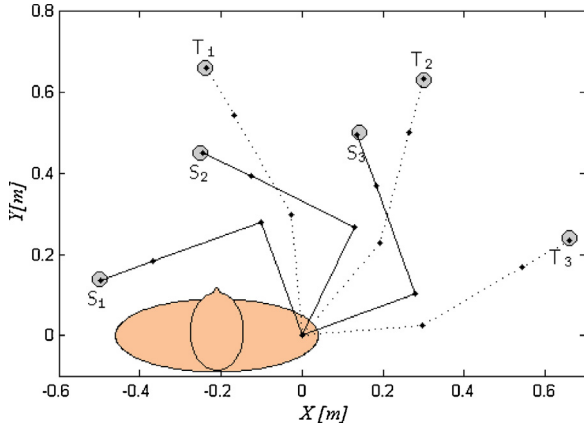


Fig. 3 – Schematic illustration of initial (solid lines) and final arm postures (dotted lines) described in Table 4. Arm postures illustrate boundary conditions of trajectories described in Table 5.

postures with shoulder extensions of 15°, 60° and 105° referred as the S_1-T_1 , S_1-T_2 and S_1-T_3 , respectively. Similarly, part B represents those with shoulder flexion to 30° and extension to 15° and 60° referred as the S_2-T_1 , S_2-T_2 and S_2-T_3 , respectively, and those with flexion to 75° and 30° and extension to 15° as the S_3-T_1 , S_3-T_2 and S_3-T_3 , respectively in the part C. We also calculated the distances between selected points. Furthermore, the important parameter for dynamic optimization is

the movement duration of each trajectory, which was also taken from the results of experiment trials [4].

2.3. Optimization method

The optimization problem was defined to find the optimal point-to-point movement with the appropriate cost functional (performance index) – see Appendix A. In the case of comparison with the experimental data, the arm muscles were excluded from the model, while in the case of simulating the muscle tightness conditions, the flexor muscles (*pectoralis major*, *brachialis* and *biceps brachii*) were included for simulating the muscle tightness. The principle of our optimization method is based on the dynamics of the motion of arm in intracorporal space. We used the concept from the field of optimal control [16] that is dominant in attempts to explain features of the arm movements. To formulate the optimization problem for the dynamical system, given in the general form

$$\dot{x} = f(x, \tau, t), \tag{17}$$

we first need to reduce the order of nonlinear dynamic equations, obtained from (3). The system of two second-order differential equations (3) can be reformulated and inverted as a system of four first-order equations:

$$\begin{aligned} \dot{\omega} &= \omega \\ \dot{\omega} &= M^{-1}(\tau + \tau_{muscles} - C\omega - B\omega), \end{aligned} \tag{18}$$

Table 5 – Kinematic profiles of all nine trajectory combinations, divided into A–C parts. The duration was taken from the results of Suzuki et al. experiment trials and the direction (flexion or extension) with magnitude of shoulder (sh) and elbow (el) joint motion was described.

	Trajectory	Distance	Duration	Direction		Magnitude	
				sh	el	sh	el
	start → end	[m]	[s]				
A	$S_1 \rightarrow T_1$	0.58	0.72	ext	ext	15°	65°
	$S_1 \rightarrow T_2$	0.94	0.83	ext	ext	60°	65°
	$S_1 \rightarrow T_3$	1.16	0.90	ext	ext	105°	65°
B	$S_2 \rightarrow T_1$	0.21	0.60	flex	ext	30°	65°
	$S_2 \rightarrow T_2$	0.58	0.72	ext	ext	15°	65°
	$S_2 \rightarrow T_3$	0.93	0.83	ext	ext	60°	65°
C	$S_3 \rightarrow T_1$	0.41	0.66	flex	ext	75°	65°
	$S_3 \rightarrow T_2$	0.21	0.60	flex	ext	30°	65°
	$S_3 \rightarrow T_3$	0.58	0.72	ext	ext	15°	65°

where θ denotes joint angles, ω angular velocities, τ joint torques and $\tau_{muscles}$ joint torques due to passive muscle forces. The state vector is then

$$x = [\theta_1 \ \theta_2 \ \omega_1 \ \omega_2]^T, \tag{19}$$

with the boundary conditions given by (20). The boundary conditions of joint angles are specified at the initial ($t=0$) and final ($t=t_f$) arm postures, shown in Table 4, while the angular velocities are equal to zero in those postures.

$$\begin{aligned} x(0) &= [\theta_{10} \ \theta_{20} \ \omega_{10} \ \omega_{20}]^T \\ x(t_f) &= [\theta_{1f} \ \theta_{2f} \ \omega_{1f} \ \omega_{2f}]^T. \end{aligned} \tag{20}$$

Before starting the process of solving the two-point boundary value problem, the initialization is needed to set the human arm parameters, the boundary conditions and the torque estimation. To determine the estimated torques, we first set the estimated hand path from start to end point, which was initially defined as a straight line trajectory in the Cartesian coordinates. The tangential velocity is bell-shaped with a single peak. Given this information and the duration of the movement t_f , the trajectory of the hand is specified in its entirety. Assuming the movement to start and end with zero velocity and acceleration, the following expressions for hand trajectory are obtained with the fifth-order polynomial in time:

$$\begin{aligned} x_h(t) &= x_0 + (x_0 - x_f)(-6T^5 + 15T^4 - 10T^3) \\ y_h(t) &= y_0 + (y_0 - y_f)(-6T^5 + 15T^4 - 10T^3), \end{aligned} \tag{21}$$

where $T = t/t_f$, (x_0, y_0) are the initial hand position coordinates at $t = 0$, and (x_f, y_f) are the final hand position coordinates at $t = t_f$. The estimated hand trajectory $(x_h(t), y_h(t))$ is then transformed into joint space by using inverse kinematics – (2) including corresponding derivatives of the joint angles $\dot{\theta}$ and $\ddot{\theta}$. Finally, the estimated torques $\tau(t)$, used as an initial guess for the optimization process, are calculated via inverse dynamics (3).

Dynamic optimization requires definition of a criterion function which describes the objective of the movement. The criterion function is expressed mathematically as a time integral of a performance index, which in general may depend on the system inputs, outputs and internal variables $L = L(x, u, t)$. In our case, a minimum torque trajectory is planned, where the torques τ required by each joint becomes the smallest, thus the criterion function has the following form

$$J = \int_0^{t_f} \tau^T \tau dt. \tag{22}$$

To find the optimal trajectory, where criterion function is satisfied, we use the first-order gradient algorithm. This method is characterized by iterative algorithm for improving estimates of the (un)specified initial or terminal conditions. A first-order gradient algorithm used for solving this optimization problem is presented step by step in Appendix B.

The projection of the optimal trajectory given by joint angles to a feature space was done by forward kinematics via (1). The velocity vectors of the optimal trajectory was also calculated with the use of Jacobian matrix that transforms the

internal to external coordinates – in our case the angular velocity to the hand velocity vectors. The relation is given by

$$\begin{bmatrix} \dot{x}_h \\ \dot{y}_h \end{bmatrix} = \begin{bmatrix} -L_1 \sin \theta_1 - L_2 \sin(\theta_1 + \theta_2) & -L_2 \sin(\theta_1 + \theta_2) \\ L_1 \cos \theta_1 + L_2 \cos(\theta_1 + \theta_2) & L_2 \cos(\theta_1 + \theta_2) \end{bmatrix} \begin{bmatrix} \dot{\theta}_1 \\ \dot{\theta}_2 \end{bmatrix}. \tag{23}$$

To calculate the trajectory velocity profile, (24) was used.

$$v(t) = \sqrt{\dot{x}_h^2 + \dot{y}_h^2} \tag{24}$$

2.4. Model evaluation

To compare predicted trajectories obtained by the optimization and the experimental data, we investigated correlation of the resulting trajectories and the velocity profiles. Various definitions of trajectory curvature are defined in the literature. We used following five curvature indexes: Normal Curvature (NC), Maximum Curvature (MxC), Medium Curvature (MdC), Total Curvature (TC), described in [17], and Whole deviation (W), defined by [18]. NC is defined as a ratio of the curvilinear abscissa to the minimum Euclidean distance between the starting and ending point, where the numerator represents the length of carried out trajectory, while the denominator is the minimum distance between the selected points – Eq. (25) and Fig. 4a.

$$NC = \frac{\sum_{i=1}^{N-1} \sqrt{dx_i^2 + dy_i^2}}{\sqrt{(x_f - x_0)^2 + (y_f - y_0)^2}} \tag{25}$$

MxC (Fig. 4b) and TC (Fig. 4d) are defined as a maximum and average value of all distances from the points defining the trajectory and the straight line defining the minimum distance. Similar curvature index is MdC (Fig. 4c), which is the distance from the executed trajectory and the straight line evaluated at half way. W (Fig. 4e) represents an area bounded between the executed trajectory and the straight line. It is also concerned with the direction in which the trajectory is curved, meaning that if the trajectory is curved to the right relatively to the vector from start to end, the area is given a positive sign, otherwise it is negative. For quantifying the tangential velocities of all predicted trajectories we first normalized the movement duration and the velocity profile. In order to compare the velocity profiles, the experimental velocity profiles were averaged and thus regarded as the reference profile. As a comparison of the predicted and experimental velocity profiles we used i.e. similarity index (SI), which is defined as a ratio of the two compared velocity profiles' intersection (minimum common area) to its union (whole area) as shown in Fig. 4f. Unlike the dissimilarity index (DI) described by [5], the similarity index is $(1 - DI)$. Furthermore, according to the calculated curvature indexes we examined the relation between the predicted and experimental data using correlation coefficient. If the curvature indexes of the experimental trajectories completely corresponded to the predicted trajectories, the slope of the regression line fitted by the least-squares method would be 1.0, and the correlation coefficient would be 1.0. The correlation coefficient is given by (26).

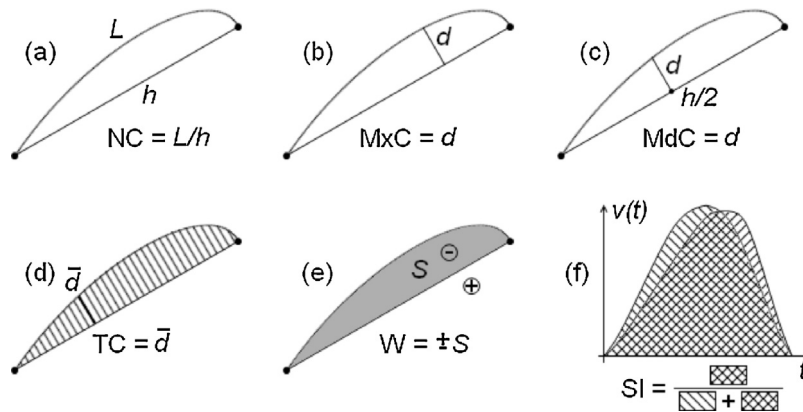


Fig. 4 – Comparison parameters explaining trajectory curvature and its velocity profile. Five different curvature indexes were used: (a) Normal Curvature (NC) – ratio of the executed trajectory length L to the straight line connecting the starting and ending point h ; (b) Maximum Curvature (MxC) – maximum distance between L and h ; (c) Medium Curvature (MdC) – distance between L and h evaluated in $h/2$; (d) Total Curvature (TC) – mean value of all the distances d between L and h ; and (e) Whole deviation (W) – signed area between L and h . For quantification of deviation of the velocity profile we used the similarity index (SI) – ratio of the two compared velocity profiles' intersection to its union (f).

$$r = \frac{\sum_{i=1}^N (x_i - \bar{x})(y_i - \bar{y})}{\sqrt{\sum_{i=1}^N (x_i - \bar{x})^2} \sqrt{\sum_{i=1}^N (y_i - \bar{y})^2}} \quad (26)$$

3. Results

3.1. Comparison with experimental data

Fig. 5 illustrates the iterative search of an optimal trajectory during the optimization process. The upper left graph shows the trajectory S_1-T_1 , where it curved to the left side of the initial straight line. According to the optimal trajectory curvature, the velocity profile became slightly different. The initial guess for the dynamic optimization was the minimum jerk trajectory, which defines bell-shaped velocity profile, but here it turns out to be more U-shape with the peak moved slightly to the right. This velocity profile is shown from the upper right graph in Fig. 5. The lower left graph shows the corresponding shoulder τ_1 and elbow τ_2 torques, which were minimized according to the optimization criterion (22). The lower right graph shows the convergence function of the first-order gradient algorithm used for numerical searching. To satisfy the optimality conditions, the algorithm needed about 300 iterations on average for all nine examined trajectories.

The results of dynamic optimization of the human arm trajectory planning with the minimum torque criterion compared with the experimental trials made by Suzuki et al. [4], are shown in Figs. 6–8. Fig. 6 illustrates the hand trajectories starting from the positions S_1 , S_2 and S_3 , respectively, to all ending positions. There are three trajectory profiles in our comparison: shortest, intermediate and long trajectories. The shortest hand trajectories (S_2-T_1 from Fig. 6B and S_3-T_2 from Fig. 6C) are nearly straight, whereas the intermediate hand trajectories (S_1-T_1 , S_1-T_2 from Fig. 6A, S_2-T_2 , S_2-T_3 from Fig. 6B and S_3-T_1 , S_3-T_3 from Fig. 6C) are curved,

while the longest hand trajectory (S_1-T_3 from Fig. 6A) is highly curved [4]. Fig. 7 illustrates the velocity profiles of all nine trajectories with the comparison of the experimentally obtained results. Gray-filled area represents a set of all experimental velocity profiles, which were obtained by [4], while dashed line shows the average of this area and was used for the reference velocity profile. Fig. 8 shows the relation between the mean velocities and the peak velocity times of each predicted trajectory. The peak velocities were normalized with respect to the movement duration expressed as a percentage, and the mean velocities were calculated for each predicted trajectory. The results show that in the case of slower movements, the peak velocity moved toward the beginning of the movement, and toward the end in the case of slightly faster movements.

As these figures show, there is a good qualitative and quantitative match between the predicted and experimental trajectories. The curvature indexes as a comparison calculation between the predicted and experimental data showed considerable similarities. They reveal significant positive correlations, which are represented in graphs in Fig. 9. The slopes of the regression line fitted by the least-squares method were 1.25, 1.04, 1.03, 1.04 and 1.02 for the curvature indexes NC, MxC, MdC, TC and W, respectively. All slopes were almost 1 except in the case of predicted-experimental NC, where the slope was a little higher. The corresponding correlation coefficients were 0.9861 ($p < 10^{-5}$), 0.9985 ($p < 10^{-9}$), 0.9983 ($p < 10^{-9}$), 0.9974 ($p < 10^{-8}$) and 0.9993 ($p < 10^{-10}$). Referring to the predicted and the reference velocity profile, similarity indexes were calculated for each pair of the trajectories (predicted and experimental). The lower right graph in Fig. 9 shows the similarity indexes of all nine velocity profiles. The average value of similarity indexes was $81 \pm 5\%$. Also, it could be seen that the peak velocities of predicted data were moved either to left or right from the 50% of movement duration.

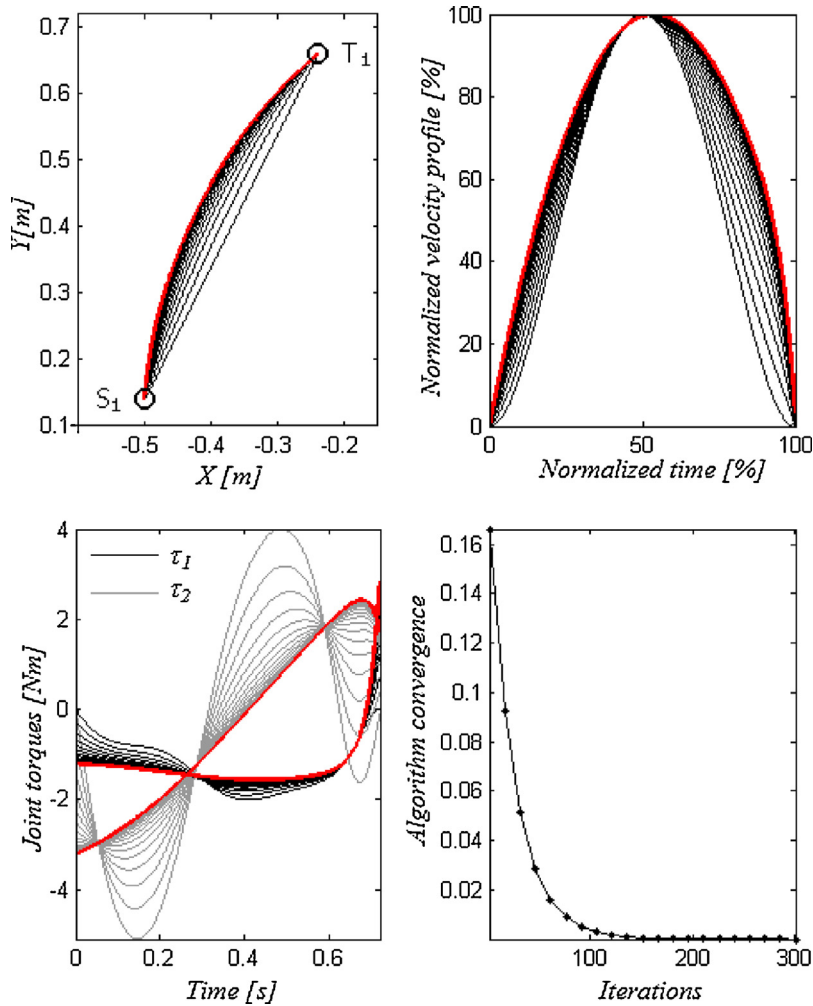


Fig. 5 – Iterative searching of the optimal trajectory between points S_1 and T_1 . The arm trajectory was curving to one side of the initial straight line (upper left graph). The tangential velocity profile became more U-shape from the initial bell-shape and the peak velocity moved slightly to the right (upper right graph). The lower left graph shows the corresponding joint torques, which became as smaller as possible according to minimum torque criterion, and the lower right graph shows the convergence of the first-order gradient algorithm. The optimal solutions are colored red.

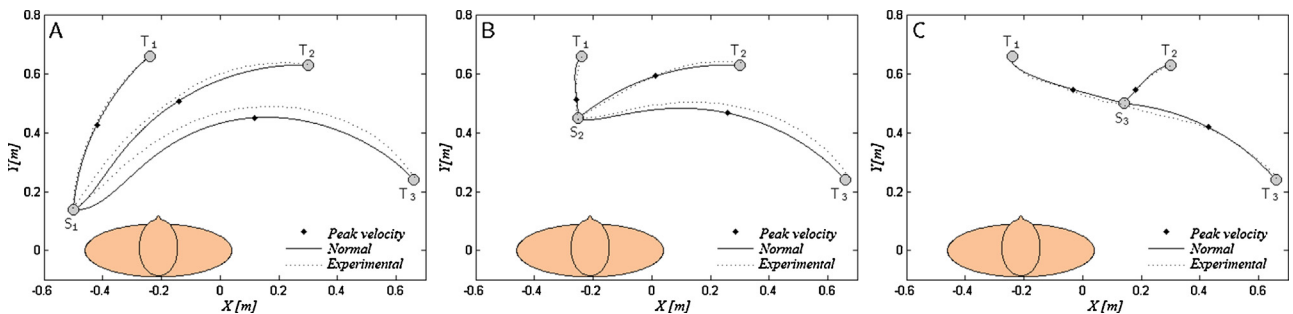


Fig. 6 – Predicted (solid lines) and experimental (dotted lines) trajectories are shown in parts A–C. The largest hand path S_1-T_3 (part A) shows higher curvature than the other two intermediate paths. The shortest hand paths S_2-T_1 (part B) and S_3-T_2 (part C) are nearly straight, while the other intermediate paths are gently curved. The predicted trajectories with a minimum torque criterion show a good matching with the experimental trajectories. The peak velocities are marked (\blacklozenge) on the predicted trajectories.

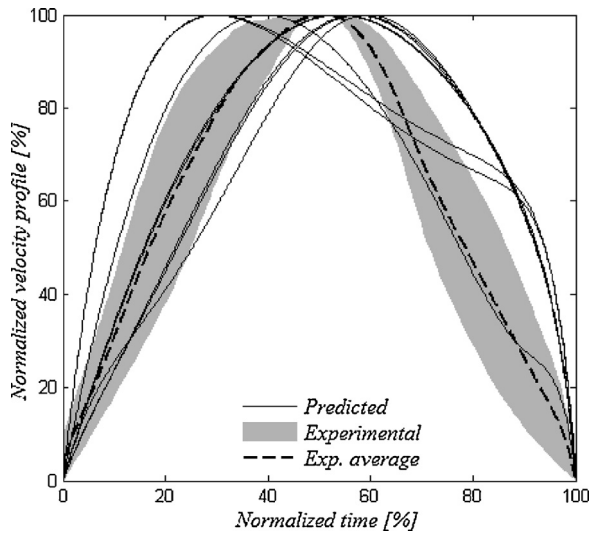


Fig. 7 – The predicted velocities (solid lines) are similar to the set of experimental velocity profiles (gray-filled area with average – dashed line).

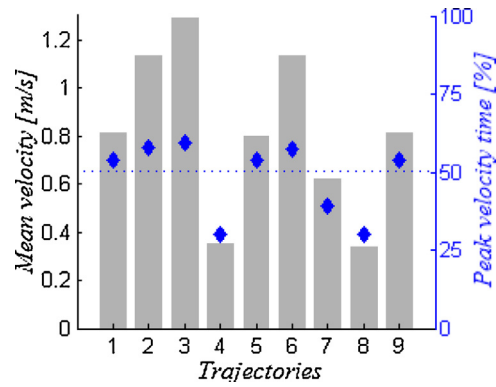


Fig. 8 – Velocity characteristics. Peak velocity times (♦) of predicted trajectories, which are normalized with respect to the movement duration expressed as a percentage. In comparison of the mean velocities (bar graph) of each trajectory, the peak velocity moved toward the beginning of the movement in the case of slower movements, and vice versa. The dotted line shows 50% of the movement duration.

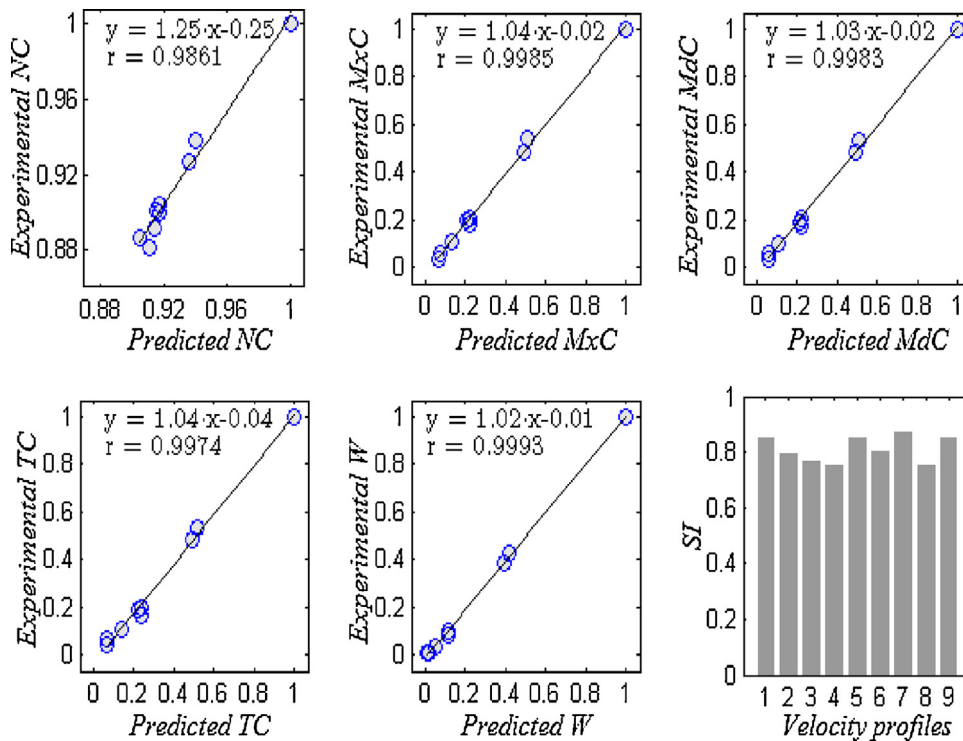


Fig. 9 – Correlations of the curvature indexes: Normal Curvature (NC), Maximum Curvature (MxC), Medium Curvature (MdC), Total Curvature (TC) and Whole deviation (W) of trajectories, and similarity indexes (SI) of velocity profiles between predicted and experimental data. Positive correlation values (r) near 1 represent good similarities between predicted and experimental trajectories, while similarity indexes of velocity profiles show approximately 81% match in average.

3.2. Optimal trajectories in case of simulated flexor muscle tightness

Fig. 10 shows the predicted optimal trajectories, where the solid trajectories represent the hand paths under the normal arm condition and the dashed lines represent the optimal

hand paths where the flexor muscles (*pectoralis major*, *brachialis* and *biceps brachii*) were included into the arm model. Besides hand paths, we also illustrated the muscle static field (described in Section 2.1.4), where different areas of static joint torques could be seen. The maximum value of static joint torques was 4.8 N m. The starting points are located in the

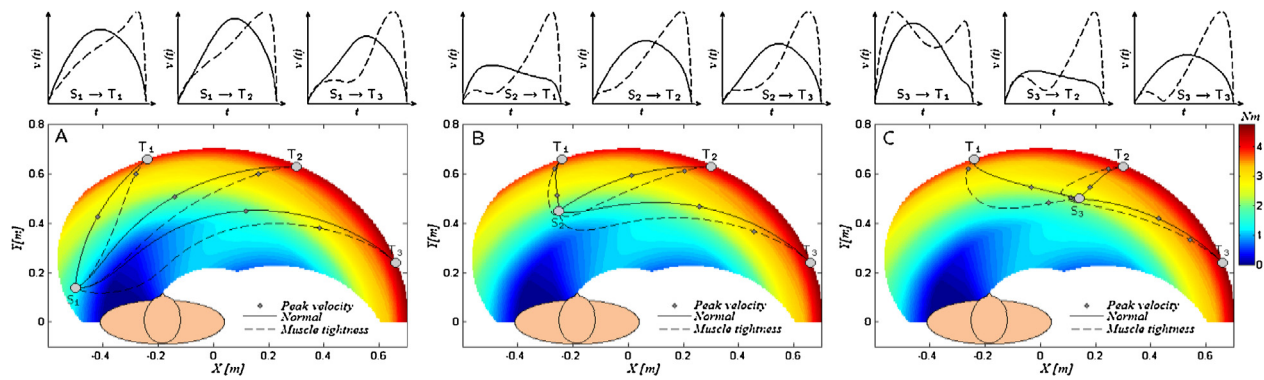


Fig. 10 – The predicted trajectories under normal conditions (solid lines) compared with predicted trajectories under muscle tightness conditions (dashed lines) are shown in parts A–C. In the background of arm’s workspace the muscle static field is shown, where it represents static joint torques due to flexor muscle tightness in each position. The velocity profiles of each pair of trajectories are shown above, where peak velocities are marked on the trajectories.

middle zone of muscle static field, while the ending points are located at the edge of the workspace, where large joint torques are needed to keep the hand in this positions. Fig. 10 (upper panel) shows the normalized velocity profiles for each pair of trajectories. It can be clearly seen that the arm’s muscle tightness trajectories are different from the normal trajectories. They are significantly differently curved with quite different velocity profile. The longest (S_1-T_3) and some intermediate hand paths (S_1-T_1 , S_1-T_2 , S_2-T_2 and S_2-T_3) under muscle tightness conditions approximately follow the minimum muscle static area at the beginning of the movement, where the hand velocities are relatively low. Eventually, as the hand approaches the ending point, the higher hand velocities are. The “muscle tightness” trajectories from part A and B in Fig. 10 have single-peaked velocity profile with the peak located in the “red” area of muscle static field. A somewhat different situation is shown in Fig. 10C, where the “muscle tightness” trajectories have two velocity peaks. The first peak position is located soon after the movement start, while the second velocity peak is already located in the “red” area of muscle static field as in the case of part A and B in Fig. 10. The first velocity peak from the “muscle tightness” trajectories S_3-T_2 and S_3-T_3 is significantly lower than the second peak, while the “muscle tightness” trajectory S_3-T_1 has two almost equal high velocity peaks – first in the early part and second in the final part of movement duration. In contrast to this trajectory all “muscle tightness” trajectories have similar velocity characteristics. In the early part of movement duration, where the muscle tightness has a relatively low impact on the movements, the hand velocities are significantly lower compared with the normal trajectories, while the more as the impact of muscle tightness increases, the higher are velocities.

4. Discussion

We have developed an optimization framework related to 2 DOF dynamic arm model that incorporates tightness of six major muscle groups and a cost function that minimizes squared torques in shoulder and elbow while performing

planar reaching movement. Optimal reaching trajectories were calculated for various starting/target points within the arm workspace that closely resembled experimental data performed in a group of neurologically intact individuals from Suzuki et al. [4]. Comparison between the results of our model and the experimental data has shown high degree of similarity. We further included some degree of muscle tightness in the flexor muscle groups in order to investigate the influence on the resulting “minimum effort” reaching trajectories. Our findings show that entirely different trajectories minimize the selected cost function in case of simulated tonic spasticity, which is predominantly the case after stroke.

The results of our study suggest that when computing optimal path for trajectories well within ROM of the arm and of short distances (such as S_2-T_1 and S_3-T_2), the selection of a cost function plays a little role. The trajectories predicted either by minimum jerk [3], by minimum torque change model [5,7,8,19,20] or by various cost functions including ones that relate to “economy of movement” in relation to point-to-point planar movements [21], would be more or less similar – nearly straight hand path with bell- or U-shaped velocity profile. However, when the distances between the starting and ending points are bigger and especially when the ending points are close to the boundaries of achievable ROM much more curved trajectories are utilized by humans as shown experimentally by Suzuki et al. [4]. Their results were corroborated by numerous simulation studies [5,6,8,19] that used optimization tools where predominantly minimum torque change cost function was minimized. Selection of a minimum torque change model implies presumed “smoothness” in the human movement which may be plausible in neurologically intact individuals. The results of our study have shown that very similar results are obtained, if a cost function, minimizing squared joint torques that relates to “economy of movement”, is utilized. This is an extent of the results from [21] where comparison between the “smoothness” and “economy of movement” cost functions in simple 1 DOF movement were practically identical. However, a selection of a minimization of squared joint torques seems to be very natural choice in the context of arm rehabilitation as this implies that such a

trajectory can be calculated where rehabilitation robot provides minimal assistance which is in line with the well accepted concept of “assistance-as-needed” rehabilitation strategy.

The results of our study show that currently used approach in rehabilitation robotics where a straight line movement between the two points in arm reaching training is supported by an impedance/admittance haptic tunnel may not be an optimal training strategy. We have demonstrated that muscle tightness plays a major role in calculation of minimum torque trajectories. For the kinematic and dynamic parameters associated with the selected reaching points the optimal trajectories are to the first approximation largely determined by the static torque field originating predominantly from simulated muscle tightness. This gives implication for a patient-specific tailoring of training trajectories that may be derived according to the experimentally identified static torque field originating from muscle tightness. The developed optimization tool proved to be stable and converged relatively fast toward optimal solution. However, the convergence of the proposed method also depends on the model nonlinearities, selection of a sufficient damping in both joints and selection of muscle tightness model. While there is little doubt that the qualitative aspects of the resulting trajectories in the case of flexor muscle tightness are in the agreement with clinical practice we will further need to experimentally verify the results of this simulation study.

5. Conclusions

Optimization model using a minimum joint torque cost function is able to predict the planar arm trajectories that closely resemble the experimental data. The optimal reaching trajectories are considerably different when muscle tightness is incorporated in the biomechanical model of planar arm reaching, which has important implications for selection of the appropriate subject-specific training trajectories supported by rehabilitation robots.

Acknowledgement

The study was supported by the grant of the Slovenian Research Agency – ARRS research programme P2-0228 and L2-2259.

Appendix A. Optimization framework

The dynamic system is described by the following system of differential equations and boundary conditions specified at a fixed terminal time:

$$\dot{x} = f(x, \tau, t), \quad (\text{A.1})$$

$$x(0) = [\theta_{10} \ \theta_{20} \ \omega_{10} \ \omega_{20}]^T, \quad (\text{A.2})$$

$$x(t_f) = [\theta_{1f} \ \theta_{2f} \ \omega_{1f} \ \omega_{2f}]^T, \quad (\text{A.3})$$

$$0 \leq t \leq t_f, \quad (\text{A.4})$$

where $x(t)$ is determined by $\tau(t)$. Consider a performance index (scalar) of the form

$$J = \int_0^{t_f} L(x, \tau, t) dt. \quad (\text{A.5})$$

The problem is to find the functions $\tau(t)$ that minimize J . If equation

$$\frac{\partial L}{\partial \tau} + [p(t) + R(t)v]^T \frac{\partial f}{\partial \tau} = 0 \quad (\text{A.6})$$

is satisfied, we have a stationary solution that satisfies the terminal constraints. This equation may be written as

$$\frac{\partial H}{\partial \tau} = 0, \quad (\text{A.7})$$

where H (the Hamiltonian) is a scalar function as follows:

$$H = L(x, \tau, t) + \lambda^T(t) f(x, \tau, t) \quad (\text{A.8})$$

and $\lambda(t)$ is a vector of *Lagrange multipliers* that consists of influence functions $p(t)$ and $R(t)$:

$$\lambda(t) = p(t) + R(t)v. \quad (\text{A.9})$$

Appendix B. Numerical solution of optimization problem: first-order gradient algorithm [16]

STEP (a) Estimate torques of shoulder and elbow joints $\tau(t)$.

STEP (b) Integrate the system equations $\dot{x} = f(x, \tau, t)$ forward with the specified initial conditions $x(0)$ and the estimate torques from STEP (a). Record $x(t)$, $\tau(t)$ and $\psi[x(t_f)]$, where

$$\psi[x(t_f)] = \begin{bmatrix} \theta_1(t_f) - \theta_{1f} \\ \theta_2(t_f) - \theta_{2f} \\ \omega_1(t_f) - \omega_{1f} \\ \omega_2(t_f) - \omega_{2f} \end{bmatrix} \quad (\text{B.1})$$

STEP (c) Determine a 4×1 vector of influence functions $p(t)$, and a 4×4 matrix of influence functions $R(t)$ by backward integration of the influence equations, using the $x(t_f)$ obtained in STEP (b) to determine the boundary conditions.

$$\dot{p} = - \left(\frac{\partial f}{\partial x} \right)^T p - \left(\frac{\partial L}{\partial x} \right)^T; \quad p(t_f) = [0 \ 0 \ 0 \ 0]^T \quad (\text{B.2})$$

$$\dot{R} = - \left(\frac{\partial f}{\partial x} \right)^T R; \quad R(t_f) = I_{4 \times 4} \quad (\text{B.3})$$

STEP (d) Simultaneously with STEP (c), compute the following integrals:

$$I_{\psi\psi} = \int_0^{t_f} R^T \frac{\partial f}{\partial \tau} \gamma^{-1} \left(\frac{\partial f}{\partial \tau} \right)^T R \ dt \quad (4 \times 4 \text{ matrix}) \quad (\text{B.4})$$

$$\begin{aligned} I_{j\psi} &= I_{\psi_j}^T \\ &= \int_0^{t_f} \left(p^T \frac{\partial f}{\partial \tau} + \frac{\partial L}{\partial \tau} \right) \gamma^{-1} \left(\frac{\partial f}{\partial \tau} \right)^T R \ dt \quad (4\text{-row vector}) \end{aligned} \quad (\text{B.5})$$

$$I_{jj} = \int_0^{t_j} \left(p^T \frac{\partial f}{\partial \tau} + \frac{\partial L}{\partial \tau} \right) \Upsilon^{-1} \left[\left(\frac{\partial f}{\partial \tau} \right)^T p + \left(\frac{\partial L}{\partial \tau} \right)^T \right] dt \quad (\text{scalar}) \tag{B.6}$$

where Υ is an 2×2 positive definite matrix with weighting parameter w :

$$\Upsilon = \begin{bmatrix} w & 0 \\ 0 & w \end{bmatrix}. \tag{B.7}$$

STEP (e) Choose values of $\delta\psi$ to cause the next nominal solution to be closer to the desired values $\psi[x(t_j)] = 0$, where $\delta\psi = -\varepsilon\psi[x(t_j)]$, $0 < \varepsilon \leq 1$. Then determine v from

$$v = -[I_{\psi\psi}]^{-1}(\delta\psi + I_{\psi j}). \tag{B.8}$$

STEP (f) Repeat STEP (a) through STEP (f), using an improved estimate of $\tau(t)$, where

$$\delta\tau(t) = -[\Upsilon(t)]^{-1} \left[\frac{\partial L}{\partial \tau} + [p(t) + R(t)v]^T \frac{\partial f}{\partial \tau} \right]^T. \tag{B.9}$$

Stop when $\psi[x(t_j)] = 0$ and $I_{jj} - I_{j\psi} I_{\psi\psi}^{-1} I_{\psi j} = 0$ to the desired degree of accuracy.

REFERENCES

[1] Abend W, Bizzi E, Morasso P. Human arm trajectory formation. *Brain* 1982;105:331-48.

[2] Morasso P. Spatial control of arm movements. *Exp Brain Res* 1981;42:223-7.

[3] Flash T, Hogan N. The coordination of arm movements: an experimentally confirmed mathematical model. *J Neurosci* 1985;5:1688-703.

[4] Suzuki M, Yamazaki Y, Mizuno N, Matsunami K. Trajectory formation of the center-of-mass of the arm during reaching movements. *Neuroscience* 1997;76:597-610.

[5] Nakano E, Imamizu H, Osu R, Uno Y, Gomi H, Yoshioka T, et al. Quantitative examinations of internal representations for arm trajectory planning: minimum commanded torque change model. *J Neurophysiol* 1999;81:2140-55.

[6] Biess A, Nagurka M, Flash T. Simulating discrete and rhythmic multi-joint human arm movements by optimization of nonlinear performance indices. *Biol Cybern* 2006;95:31-53.

[7] Uno Y, Kawato M, Suzuki R. Formation and control of optimal trajectory in human multijoint arm movement. *Biol Cybern* 1989;61:89-101.

[8] Wada Y, Kaneko Y, Nakano E, Osu R, Kawato M. Quantitative examinations for multi joint arm trajectory planning - using a robust calculation algorithm of the minimum commanded torque change trajectory. *Neural Network* 2001;14:381-93.

[9] Nagasaki H. Asymmetric velocity and acceleration profiles of human arm movements. *Exp Brain Res* 1989;74: 319-26.

[10] Kim HK, Carmenta JM, Biggs SJ, Hanson TL, Nicoletis MAL, Srinivasan MA. The muscle activation method: an approach to impedance control of brain-machine interfaces through a musculoskeletal model of the arm. *Biomed Eng (NY)* 2007;54:1520-9.

[11] Chandler RF, Clauser CE, McConville JT, Reynolds HM, Young JW. Investigation of inertial properties of the human body. AMRL Technical Report; 1975. pp. 74-137.

[12] Jensen RK. Changes in segment inertia proportions between four and twenty years. *J Biomech* 1989;22: 529-36.

[13] Hinricks RN. Regression equations to predict segmental moments of inertia from anthropometric measurements: an extension of the data of Chandler et al. (1975). *J Biomech* 1985;18:621-4.

[14] Zatsiorsky VM, Seluyanov VN. The mass and inertia characteristics of the main segments of the human body. *Biomechanics* 1983;VIII-B:1152-9.

[15] Tahara K, Luo Z, Arimoto S, Kino H. Sensory-motor control of a muscle redundant arm for reaching movements - convergence analysis and gravity compensation. In: *Intelligent Robots and Systems (IROS)*. 2005. pp. 517-22.

[16] Bryson AE, Ho YC. *Applied optimal control: optimization, estimation, and control*. New York: Taylor & Francis; 1975.

[17] Bernabucci, Conforto S, Capozza M, Accornero N, Schmid M, D'Alessio T. A biologically inspired neural network controller for ballistic arm movements. *J Neuroeng Rehabil* 2007;4:33.

[18] Osu R, Uno Y, Koike Y, Kawato M. Possible explanations trajectory curvature in multijoint arm movements. *J Exp Psychol Hum Percept Perform* 1997;23:890-913.

[19] Ohta MM, Svinin ZW, Luo S, Hosoe R, Laboissiere. Optimal trajectory formation of constrained human arm reaching movements. *Biol Cybern* 2004;91:23-36.

[20] Wolpert DM, Ghahramani Z, Jordan MI. Are arm trajectories planned in kinematic or dynamic coordinates? An adaptation study. *Exp Brain Res* 1995;103:460-70.

[21] Nelson WL. Physical principles for economies of skilled movements. *Biol Cybern* 1983;46:135-47.